REPORT DOCUMENTATION PAGE

Form Approved
OMB No. 0704-0188

1. AGENCY USE ONLY (Leave blank)	2. REPORT DATE	3. REPORT TYPE AND DATES COVERED
	17 June 1993	Master's Thesis

4. TITLE AND SUBTITLE
Calibration of a High Frequency Monostatic Acoustic Echosounder

5. FUNDING NUMBERS

6. AUTHOR(S)
Cherry, David R.

7. PERFORMING ORGANIZATION NAME(S) AND ADDRESS(ES)
Naval Postgraduate School
Monterey, CA 93943-5000

8. PERFORMING ORGANIZATION REPORT NUMBER

9. SPONSORING/MONITORING AGENCY NAME(S) AND ADDRESS(ES)

10. SPONSORING/MONITORING AGENCY REPORT NUMBER

11. SUPPLEMENTARY NOTES
The views expressed in this thesis are those of the author and do not reflect the policy or the position of the Department of Defense or the U.S. government.

12a. DISTRIBUTION/AVAILABILITY STATEMENT
Approved for public release; distribution is unlimited.

12b. DISTRIBUTION CODE

13. ABSTRACT *(Maximum 200 words)*

Atmospheric turbulence degrades a coherent laser beam when it propagates through the atmosphere. Measurements of the distribution of atmospheric turbulence provide insight into the underlying mechanisms that produce optical turbulence and suggest possible means to overcome or circumvent the effects of such turbulence. A variety of acoustic, optical and thermal probe instruments provide measurements of atmospheric turbulence. Of these, the acoustic echosounder can measure atmospheric density and velocity irregularities. During the course of previous work, questions arose concerning the calibration of the NPS echosounder. The echosounder appears to detect a higher level of atmospheric turbulence than do other instruments used at the same altitude. This resulting overestimation of atmospheric turbulence could significantly influence programs such as the Advanced Electro-Optic Site (AEOS), a proposed 4 m telescope to be built in Hawaii.

This thesis will attempt to identify key components contributing to the sounder calibration including the transducer transmit and receive efficiencies as well as their dependence on pressure and atmospheric density. Additionally a modified acoustic echosounder equation will be developed which more accurately profiles the atmospheric turbulence measured by such a sounder.

14. SUBJECT TERMS	15. NUMBER OF PAGES
acoustic echosounder, atmospheric turbulence,	56
	16. PRICE CODE

17. SECURITY CLASSIFICATION OF REPORT	18. SECURITY CLASSIFICATION OF THIS PAGE	19. SECURITY CLASSIFICATION OF ABSTRACT	20. LIMITATION OF ABSTRACT
UNCLASSIFIED	UNCLASSIFIED	UNCLASSIFIED	SAR

Approved for public release; distribution is unlimited.

Calibration of
a High Frequency
Monostatic Acoustic Echosounder

by

David R. Cherry
Major, United States Army
B.S., Florida State University, 1977

Submitted in partial fulfillment
of the requirements for the degree of

MASTER OF SCIENCE IN PHYSICS

from the

NAVAL POSTGRADUATE SCHOOL
June 1993

ABSTRACT

Atmospheric turbulence degrades a coherent laser beam when it propagates through the atmosphere. Measurements of the distribution of atmospheric turbulence provide insight into the underlying mechanisms that produce optical turbulence and suggest possible means to overcome or circumvent the effects of such turbulence. A variety of acoustic, optical and thermal probe instruments provide measurements of atmospheric turbulence. Of these, the acoustic echosounder can measure atmospheric density and velocity irregularities. During the course of previous work, questions arose concerning the calibration of the NPS echosounder. The echosounder appears to detect a higher level of atmospheric turbulence than do other instruments used at the same altitude. This resulting overestimation of atmospheric turbulence could significantly influence programs such as the Advanced Electro-Optic Site (AEOS), a proposed 4 m telescope to be built in Hawaii.

This thesis will attempt to identify key components contributing to the sounder calibration including the transducer transmitting and receiving efficiencies as well as their dependence on pressure and atmospheric density. Additionally a modified acoustic echosounder equation will be developed which more accurately profiles the atmospheric turbulence measured by such a sounder.

TABLE OF CONTENTS

I. INTRODUCTION 1

II. BACKGROUND 4

A. ATMOSPHERIC TURBULENCE 4

1. Refractive Turbulence Structure Parameter 4

2. Temperature Structure Parameter 5

3. Spatial Coherence Length 6

B. THE ACOUSTIC ECHOSOUNDER 7

III. DISCUSSION 11

A. PREVIOUS WORK 11

1. Transducer Efficiency 11

2. Effective Aperture Factor 12

B. FIELD MEASUREMENTS 13

1. Advanced Electro-Optic Site (AEOS) 13

2. Starfire Optical Range (SOR) 16

C. ECHOSOUNDER OPERATION 20

1. Receiving Efficiency 20

2. Transmitting Efficiency 22

3. Altitude Dependence 25

4. Modified Echosounder Equation 28

IV. EXPERIMENTAL RESULTS 31

A. RECEIVING EFFICIENCY 31

B. TRANSMITTING EFFICIENCY 32

C. ALTITUDE DEPENDENCE 36

D. MODIFIED ECHOSOUNDER EQUATION 40

V. CONCLUSIONS AND RECOMMENDATIONS 44

A. CONCLUSIONS 44

B. RECOMMENDATIONS 46

LIST OF REFERENCES 47

INITIAL DISTRIBUTION LIST 49

ACKNOWLEDGEMENTS

I would like to express my deepest gratitude and heartfelt thanks to my family who, through their assistance and encouragement, made this work possible. First and foremost I would like to thank my friend, partner and wife, Cathy. Without her love, support and encouragement during the past two and one half years, I doubt I ever would have been able to accomplish this task. Also I would like to thank my sons, David and Rande, who managed to never let me forget what was really important. It is to these really special people in my life that I would like to dedicate this work.

I. INTRODUCTION

Turbulence degrades a coherent laser beam when it propagates through the atmosphere. Atmospheric irregularities randomize the amplitudes and phases of the electromagnetic waves as they propagate through these turbulent regions. The result is that an initially focused beam is defocused, which reduces the irradiance delivered to the target.

Measurements of the distribution of atmospheric turbulence provide insight into the underlying mechanisms that produce optical turbulence and suggest possible means to overcome or circumvent the effects of such turbulence.

A variety of acoustic, optical and thermal probe instruments provide measurements of atmospheric turbulence. Of these, the acoustic echosounder can measure atmospheric density and velocity irregularities resulting from air currents, temperature inversions, humidity variations, mechanical turbulence and other causes.

Walters has probed the atmosphere, quantitatively characterizing its turbulence, over the last decade. He has made extensive measurements in the mountainous area in the vicinity of White Sands, New Mexico [Ref. 1].

Working with Walters, Weingartner [Ref. 2] and Wroblewski [Ref. 3] built and tested a 25 element 5 kHz planar array acoustic echosounder. Moxcey

[Ref. 4] later modified this design by placing the drivers closer together into a 19 element, hexagonal, close-packed array. This modification increased the acoustic power in the main lobe and suppressed the side lobes. The result was an extremely effective low altitude echosounder that was less expensive, more portable and had better side lobe reduction than previous monostatic sounders.

During the course of the previous work, questions arose concerning the calibration of the echosounder. The echosounder appears to detect a higher level (by a factor of almost four) of atmospheric turbulence than do other instruments (e.g., high speed temperature probes) used at the same altitude.

The resulting overestimation of atmospheric turbulence could significantly influence programs such as the Advanced Electro-Optic Site (AEOS), a proposed 4 m telescope to be built on Mount Haleakala, Maui, Hawaii. For AEOS it is crucial to find the best design compromise, to reduce atmospheric turbulence, either naturally or by building a telescope support pedestal above the turbulent layer. An overestimation of turbulence would require a pedestal higher than is actually necessary to get above the turbulent layer, consequently wasting money.

This thesis will attempt to identify key components contributing to the acoustic sounder calibration, including the transducer transmitting and receiving efficiencies, as well as their dependence on pressure and atmospheric density. Measurements made in the NPS anechoic chamber will be compared with field calibration measurements made at the Starfire Optical Range against three

differential-temperature probes mounted on a tower. A modified acoustic echosounder equation will be developed that utilizes transducer calibration parameters measured in the laboratory.

II. BACKGROUND

A. ATMOSPHERIC TURBULENCE

Random phase perturbations occur as optical waves propagate through the atmosphere. These small scale phase variations cause the light beam to diverge, reducing the irradiance on a target. Atmospheric density fluctuations carried by the turbulent velocity field cause these optical phase perturbations by affecting the local index of refraction. Temperature fluctuations create such density variations, which can occur over scales anywhere from tens of meters in size down to sub-centimeter ranges.

These phenomena degrade the resolution of both earth-bound observation facilities and laser platforms. The following two parameters characterize this degradation: the refractive turbulence structure parameter, C_n^2, and the spatial coherence length of the atmosphere, r_o. These parameters are most variable and inhomogeneous at the interface between stratified atmospheric layers. This is particularly relevant near the earth's surface.

1. Refractive Turbulence Structure Parameter

The refractive turbulence structure parameter, C_n^2, is the mean-squared statistical average of the difference between the indices of refraction at two points, scaled by the points' separation. Tatarski [Ref. 5] includes a detailed discussion of this parameter, defined as

$$C_n^2 = \frac{\langle (n_1 - n_2)^2 \rangle}{r_{12}^{2/3}} \quad , \qquad (1)$$

where $\langle\ \rangle$ signifies an ensemble average, n_1 and n_2 are the indices of refraction at points 1 and 2 respectively, and r_{12} is the separation between points 1 and 2 in the atmosphere. C_n^2 is a measure of the local variability in refractive index, and it provides the starting point in analyzing the resulting optical turbulence. It is important to note that the presence of significant velocity turbulence does not imply an appreciable degree of optical turbulence, and vice versa [Ref. 6]. Unfortunately, C_n^2 is a difficult parameter to measure directly. It is easier to make direct measurements of another atmospheric structure parameter, C_T^2.

2. Temperature Structure Parameter

The temperature structure parameter, C_T^2, is the analogous measure of temperature fluctuations between two points in space

$$C_T^2 = \frac{\langle (T_2 - T_1)^2 \rangle}{r_{12}^{2/3}} \quad , \qquad (2)$$

where T_1 and T_2 are the temperatures at points 1 and 2 respectively and r_{12} is defined as in Equation (1). As will be discussed in the following section, an acoustic echosounder measures this parameter indirectly. For optical wavelengths, Tatarski [Ref. 5] developed the following relationship between C_n^2 and C_T^2:

$$C_n^2 = \left(\frac{79 \times 10^{-6} P}{T^2}\right)^2 C_T^2 \quad , \qquad (3)$$

where P is the atmospheric pressure in millibars, and T is the temperature in kelvin. Equation (3) ignores a contributing factor that depends on the water vapor concentration, that is important quantifying the effects of turbulence on the propagation of microwave radiation.

3. Spatial Coherence Length

As previously mentioned, the spatial coherence length, r_o, introduced by Fried [Ref. 7], is an important optical turbulence parameter. It is a measure of the spatial correlation of the electric fields of the optical beam, measured in a plane perpendicular to the direction of propagation. r_o is a function of the magnitude of the integrated optical turbulence and depends on the integral of C_n^2 over the propagation path in question. For a plane wave,

$$r_o = 2.1 \left[1.46 k^2 \int_0^L C_n^2 (z)\, dz\right]^{-3/5} \quad , \qquad (4)$$

where k is the wave number ($2\pi/\lambda$) and L is the optical path length. Coherence lengths for vertical beam propagation vary widely between observation sites. Coherence length values can range from a few centimeters at a poor site to around 30 cm at a world-class site.

B. THE ACOUSTIC ECHOSOUNDER

Acoustic echosounders transmit a pulse of acoustic energy to detect atmospheric density variations in much the same way as a shipborne sonar detects the presence of a submarine. The density structure of the atmosphere scatters a portion of the transmitted energy back to the echosounder. The power returned from these turbulent structures, P_R, is proportional to the power transmitted, P_T. The echosonde equation, also known as the radar equation, has been adapted by Neff [Ref. 8], based upon work by Tatarski [Ref. 5], Little [Ref. 9] and Hall [Ref. 10], to the operation of an echosounder:

$$\frac{P_R}{E_R} = [P_T E_T]\ [e^{-2\alpha R}]\ [\sigma_o(R, f)]\ [\frac{c\tau}{2}]\ [\frac{A}{R^2} G] \qquad (5)$$

with,

- P_R/E_R is the received acoustic power, where P_R is the measured electrical power and E_R is the efficiency of conversion from received acoustic power to electrical power.
- $P_T E_T$ is the radiated acoustic power, where P_T is the electrical power applied to the transducer and E_T is the efficiency of conversion of electrical driving power to radiated acoustic power.
- $e^{-2\alpha R}$ is the round trip power loss resulting from attenuation by air, where α is the average attenuation (m^{-1}) to the scattering volume at range R (m).
- $\sigma_o(R,f)$ is the acoustic scattering cross-section per unit volume; that is, the fraction of incident power backscattered per unit distance into a unit solid angle at frequency f (Hz).
- $c\tau/2$ is the maximum effective scattering volume thickness, where c is the local speed of sound (ms^{-1}) and τ is the pulse length (s).

- AG/R^2 is the solid angle subtended by the antenna aperture A (m^2) from the scattering volume, modified by an effective aperture factor G, arising from the antenna's directivity and geometry.

As mentioned previously, the acoustic echosounder measures atmospheric turbulence, C_T^2, values via the scattering cross-section, σ. Tatarski [Ref. 5] shows that the backscattering cross-section is proportional to C_T^2 through the following relationship,

$$\sigma(R, f) = 0.0039\, k^{1/3} \left(\frac{C_T^2}{T^2}\right) \qquad (6)$$

where,

- T is the absolute temperature (K),
- k is the acoustic wave number (m^{-1}),
- λ is the acoustic wavelength (m).

This is the case only for backscattered acoustic energy, that is, energy which is scattered through an angle of 180 degrees. For other angles, the amount of energy scattered depends upon the velocity structure parameter of the atmosphere [Ref. 5]. Combining Equations (5) and (6), and solving for C_T^2 gives,

$$C_T^2 = \left[\frac{2}{0.0039\, E_T E_R A G}\right] \frac{T^2}{k^{1/3}} \left[\frac{P_R}{c\tau P_T}\right] R^2 e^{-2\alpha R} \quad . \qquad (7)$$

Several of the factors appearing in Equation (7), such as P_T, E_T, E_R and G are difficult to determine accurately. Therefore, a certain degree of error exists

with an acoustic sounder that must be dealt with when calibrating such a device. One calibration technique involves operation of an acoustic echosounder in the vicinity of a tower that has high speed temperature probes mounted at known heights. The measurements from the temperature probes are compared to the echosounder data. Although, straightforward, this procedure does not allow for extrapolation of the calibration to other locations, particularly when significant atmospheric density changes occur. Reference 11 discusses echosounder calibration in detail.

The heart of the NPS echosounder is an array of 19 Motorola KSN 1005A piezoelectric speakers mounted in a hexagonal shaped array. These speakers were chosen for their resonance properties and high transmission and receiving efficiencies. The complete echosounder system is shown in Figure 1.

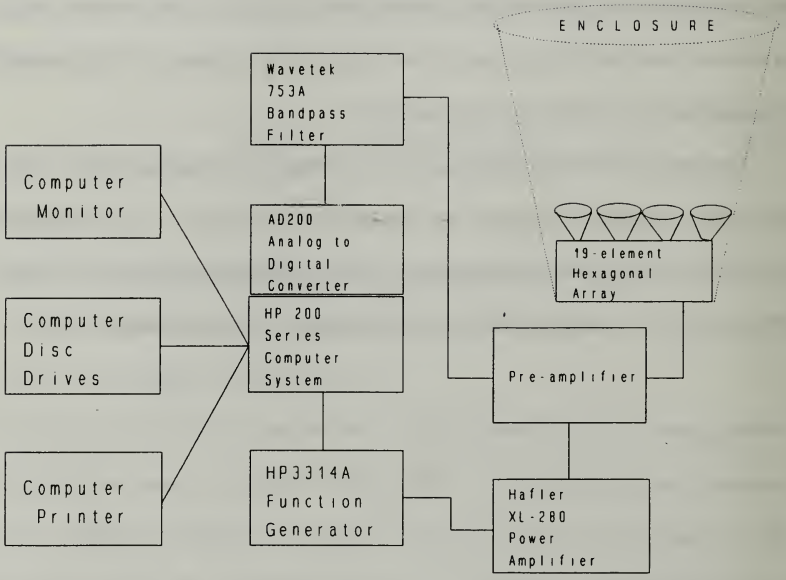

Figure 1. The Acoustic Echosounder System.

III. DISCUSSION

A. PREVIOUS WORK

1. Transducer Efficiency

The acoustic echosounder is an excellent tool for probing the lower troposphere, however it has a limited range (~200 m) that depends on the acoustic frequency used and on atmospheric attenuation. The system estimates atmospheric turbulence by measuring the absolute acoustic energy scattered by the atmosphere. The transducer transmitting and receiving efficiencies must be known in order to measure the returned power. Transducer efficiency can typically range anywhere from a few percent [Ref. 8] to 25 percent [Ref. 12].

The echosounder operation is frequency-dependent. Its ability to measure the spatial resolution of temperature structures increases at higher operating frequencies, but atmospheric attenuation increases exponentially with frequency as well. The Motorola KSN 1005A speakers used in the hexagonal array have a maximum response at a resonant frequency of 5000 Hz. Although a lower frequency would reduce atmospheric attenuation, 5000 Hz optimizes the speaker efficiency and spatial resolution [Ref 2].

Weingartner, under Walters' supervision, assembled the first operational acoustic echosounder system. He measured the transducer

receiving efficiency, E_R, and found it to be 50 percent [Ref. 2]. This was much higher than the efficiency predicted by References 8 and 12. He was not able to measure the transmitting efficiency, E_T, so he assumed that the values for E_R and E_T were equal, with value 0.5.

2. **Effective Aperture Factor**

Weingartner's system employed a 5 x 5 (25 element) square array of transducers. He used calculations that Hall and Wescott [Ref. 10] made for the beam-shape compensation factor. Their work was based on the theoretical development by Probert-Jones [Ref. 13]. This value, 0.40, is the same as the effective-aperture factor, G, in Equation (7).

Moxcey [Ref. 4] modified the array by reducing the number of speakers from 25 to 19 and packing these transducers closer together into a hexagonal configuration. This reduced the side lobes and increased the power in the main lobe. Approximating the aperture area of the array to be equivalent to 19 times the aperture area of a single speaker having a diameter of 7.620 centimeters, one gets a value of 0.0866 m^2 for the area of the array. This is the antenna area, A, in Equation (7).

Equation (7) uses the above values for E_R, E_T, G and A. Combining these values with the constants and simplifying we get,

$$C_T^2 = 59217 \left[\frac{T^2}{k^{1/3}}\right] \left[\frac{P_R}{c\,\tau\,P_T}\right] R^2\, e^{-2\alpha R} \quad , \qquad (8)$$

for the relationship between C_T^2 and the echosounder system.

B. FIELD MEASUREMENTS

1. Advanced Electro-Optic Site (AEOS)

The Air Force is planning to build a 4 m telescope on the top of Mount Haleakala on the island of Maui in Hawaii. Turbulence will interfere with the "seeing ability" of the telescope. Previous data indicate that a pedestal can raise the telescope above the majority of the low level turbulence. This appears to be feasible since the majority of the turbulence is confined to a ~20 m level layer which hugs the contours of the mountain. Two questions are: how thick is this ground layer and how much turbulence does it contain? Also, how high does the pedestal have to be to get above this ground layer?

Measurements with an acoustic echosounder were made on three separate occasions to determine the extent of the turbulence in the ground layer. The first measurements were made by the Environmental Studies Section of the Rome Air Development Center (RADC) in August 1974 [Ref. 14]. Their echosounder did not find any significant turbulence, of sufficient strength to degrade seeing, within the range 100-1000 ft. Their data for the range 0-100 ft was inconclusive.

The second set of data reported by Mattingly [Ref. 11] were recorded during the period 26 June - 2 July 1991. He found an intensely turbulent layer within the first 80 meters above AEOS. He calculated a 30-40% improvement in both daytime and nighttime seeing quality for a 15-25 m tower.

The third set of data reported by Gast [Ref. 15] were recorded during the period 3-12 March 1992. His measurements indicated significant turbulence present in the region from 10-100 m above AEOS, although this turbulence was not as intense as that found by Mattingly [Ref. 11]. Gast found that the echosounder was reporting turbulence at a level approximately four times larger than would be expected. This was based upon the maximum value that Walters measured for the log of C_n^2, (-13.0), in the desert, at noon when atmospheric turbulence is greatest [Ref 1]. Figure 2 shows that the AEOS data exceeded this maximum value for over ten hours 20 m above the ground. However, problems in the microthermal probe electronics used for calibration make these comparisons suspect and inconclusive.

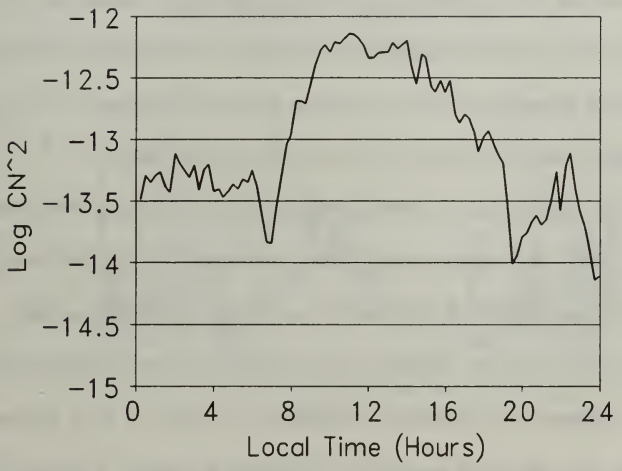

Figure 2. C_n^2 data from AEOS which shows that unmodified measurements exceed maximum expected values (-13.0) for a desert location at high noon, the most turbulent time of day.

2. Starfire Optical Range (SOR)

Measurements were conducted at the Starfire Optical Range, Kirkland Air Force Base, Albuquerque, New Mexico on two occasions. The first set of measurements took place from 28 through 30 April 1992. The calibration for these measurements, at 11.5 and 40 m altitude, was found to be invalid when it was discovered that an RMS chip inside the reference probes had a floating connection that introduced a substrate bias error. The reference probe used at 20.5 m altitude operated correctly, so those data are not suspect. The floating ground problem was discovered and corrected in July 1992.

The second set of measurements occurred during the period 5-9 September 1992. Reference probes were positioned at 11.5, 20.5 and 40 m altitudes. Figures 3 through 5 show that all probes operated correctly. This was the first time that the acoustic echosounder was compared directly with a credible independent calibration. However, a factor of four discrepancy between the two data sets was evident. Figures 3 through 5 show that the echosounder values closely resemble the tower mounted high speed temperature probes, after the echosounder data has been divided by four.

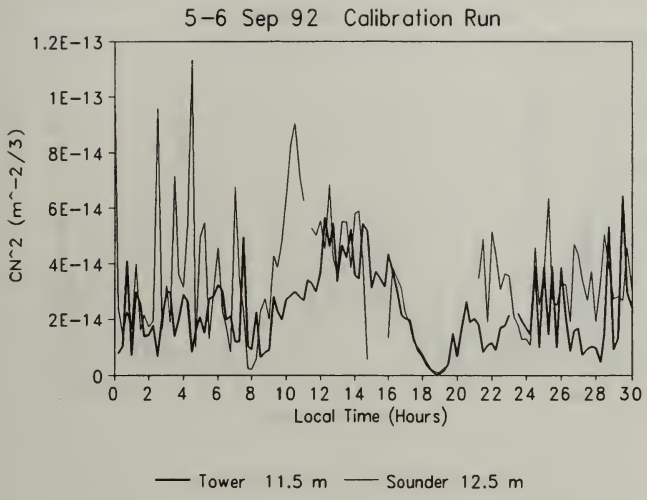

Figure 3. Echosounder data, divided by four, resembles data collected simultaneously by tower-mounted, high speed temperature probes at a similar height.

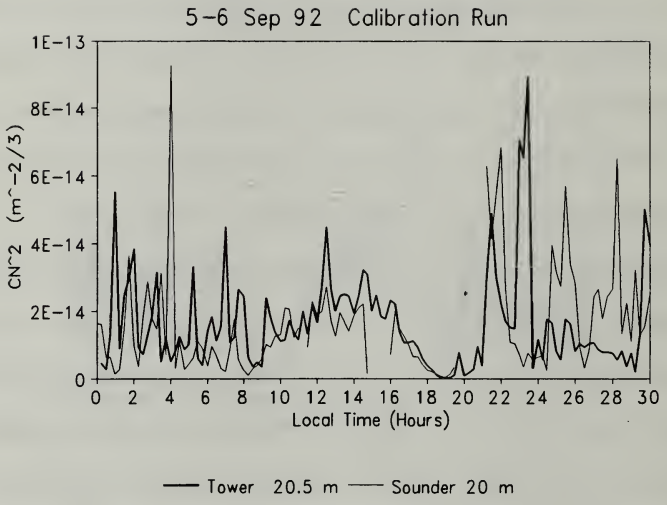

Figure 4. Echosounder data, divided by four, closely resembles data collected simultaneously by tower-mounted, high speed temperature probes at a similar height.

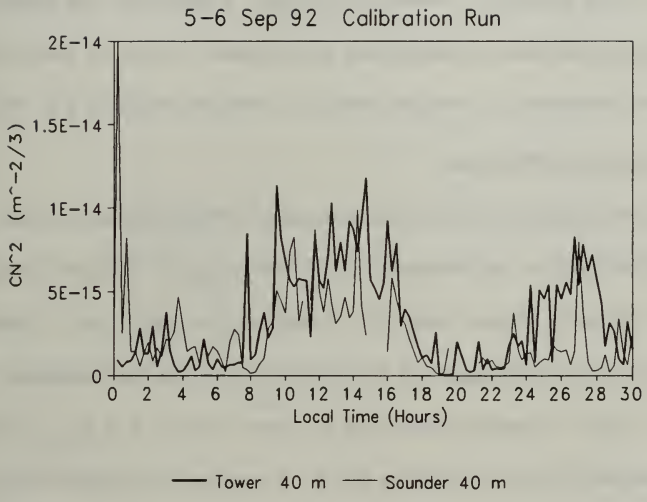

Figure 5. Echosounder data, divided by four, closely resembles data collected by tower-mounted, high speed temperature probes at a same height.

C. ECHOSOUNDER OPERATION

The echosounder can only measure atmospheric turbulence accurately when the system performance factors (i.e., E_R, E_T, P_T, G) are known and incorporated into Equation (7). These factors will be measured/calculated to determine if they are responsible for the echosounder reporting turbulence at a level four times larger than would be expected. Additionally, the transducer efficiency dependence on pressure was investigated in order to use the SOR echosounder calibration to evaluate data at a different pressure e.g., AEOS.

1. Receiving Efficiency

The receiving efficiency was measured in the NPS anechoic chamber, using a HP3314A Function Generator, a HP 3561A Dynamic Signal Analyzer, a one inch reference speaker and the 19 element hexagonal array. Figure 6 shows the experimental equipment arrangement. The function generator with a 50 ohm output impedance provided an open circuit, 1.0 volt, 5.0 kHz sinusoidal signal to a one inch dome driver. The array was aligned along the centroid of the main lobe of the reference speaker signal. The array received the transmitted acoustic signal and the HP 3561A Signal Analyzer measured the RMS amplitude of the signal.

The array was then replaced with a 1/4 inch, Cartridge Type 4135, Brüel & Kjaer (B&K), calibrated condenser microphone, with Type 2633 preamplifier. The microphone was calibrated using a B&K pistonphone, prior

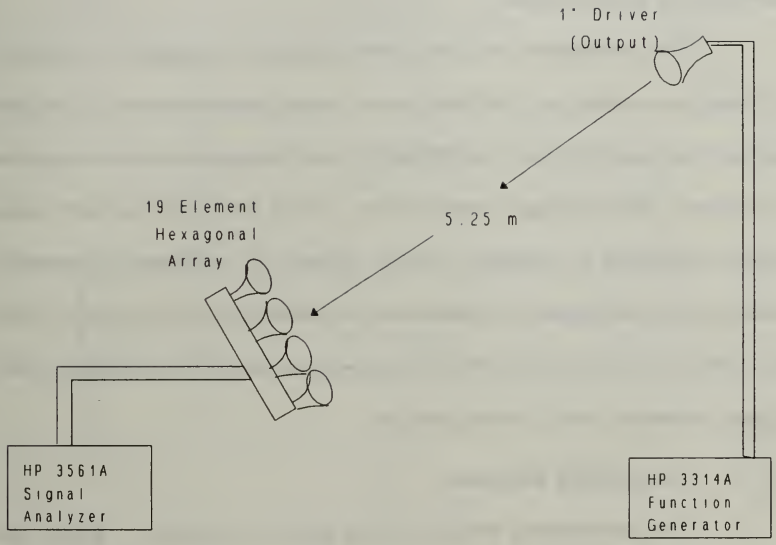

Figure 6. Receiving efficiency measurement equipment set-up inside the anechoic chamber.

to use. The pistonphone has a chamber of accurately known volume in which a piston of known area oscillates with known displacement amplitude [Ref 16]. The microphone calibration coefficient, C_{piston}, was the RMS signal voltage divided by the RMS pressure generated by the pistonphone calibration source. The measurements made with the microphone were then divided by this coefficient to scale the data.

The microphone determined the total power available for reception by the acoustic array, i.e., the total power actually ensonified within the solid angle of the acoustic array. An HP 3561A digital spectrum analyzer made the microphone, RMS voltage measurements. With the small one inch dome speaker providing a reference acoustic signal, the calibrated microphone measured the sound pressure field with the echosounder array removed. After placing the array in the sound field, the receive sensitivity was the open circuit voltage divided by the incident pressure.

2. Transmitting Efficiency

The transmitting efficiency was harder to measure. Again, this measurement was made inside the anechoic chamber. The HP3314A Function Generator generated a 1.0 V_{Peak}, 5.0 kHz, sinusoidal signal with a 50 Ω output impedance which was connected to the hexagonal array i.e., the array was used to transmit the signal this time. Figure 7 shows the experimental equipment arrangement. A 1/4 inch, Cartridge Type 4135, B&K calibrated condenser microphone, positioned on a thin rod, received the signal and passed

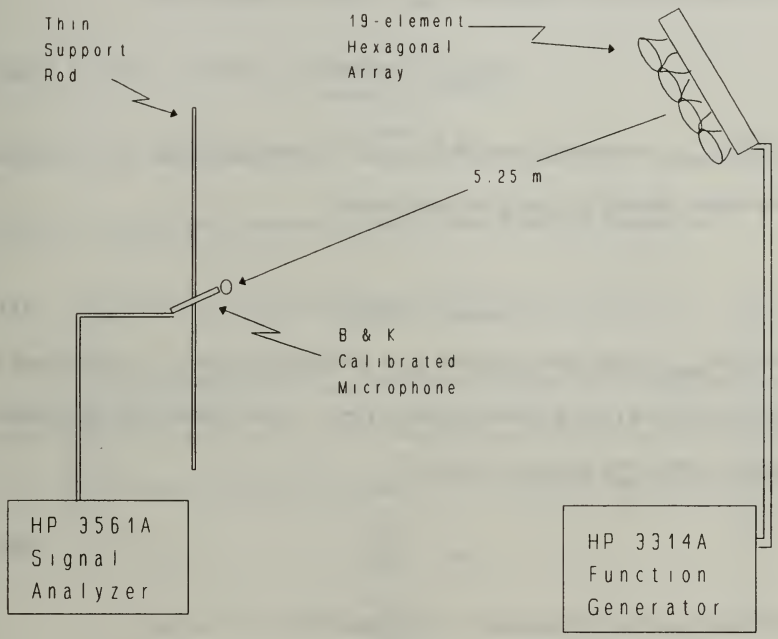

Figure 7. Transmitting efficiency measurement equipment set-up inside the anechoic chamber.

it to the signal analyzer. A signal amplitude measurement was made at the centroid of the main lobe and then again at 5 cm increments out to the first node.

These voltage measurements (V_m) were first converted to pressure using the conversion coefficient (C_{piston}) from the pistonphone

$$P_{pressure} = \frac{V_m}{C_{piston}} \quad , \tag{10}$$

where $P_{pressure}$ is the RMS pressure in pascal. This pressure was then converted to a power density (I) using the relationship

$$P_{pressure} = \sqrt{2 \rho_o c I} \quad , \tag{11}$$

where $P_{pressure}$ is the peak pressure, ρ_o is air density (kg/m^3), c is the speed of sound (m/s) and I is the power density (W/m^2). After recalling the relationship between peak and average pressure

$$P_{RMS} = \frac{P_{Peak}}{\sqrt{2}} \quad , \tag{12}$$

and inserting this into Equation (11) and solving for I we get

$$I = \frac{P_{RMS}^2}{\rho_o c} \quad . \tag{13}$$

These power densities, I, were then integrated over the surface of the acoustic beam's main lobe to find the total power, P_{total}, in the lobe, as follows:

$$P_{total} = \int I \, dx \, dy \quad . \tag{14}$$

Expressing this integral in polar coordinates

$$P_{total} = \int_0^{\rho_{max}} \int_0^{2\pi} I \rho \, d\rho \, d\theta \quad . \tag{15}$$

Since I is axially symmetric, the integral becomes

$$P_{total} = 2\pi \int_0^{\rho_{max}} I \rho \, d\rho \quad . \tag{16}$$

Simpson's method of numerical integration evaluates this integral as

$$\int_a^b f(x) \, dx \approx S = \frac{h}{3} (y_o + 4y_1 + 2y_2 + 4y_3 + \cdots + 2y_{n-2} + 4y_{n-1} + y_n) \quad . \tag{17}$$

The acoustic power, P_{total}, was then compared to the electrical input power applied to the array, P_{input}. The transmitting efficiency, E_T, was the ratio of the total acoustic input power divided by the electrical input power to the array

$$E_T = \frac{P_{total}}{P_{input}} \quad . \tag{18}$$

3. Altitude Dependence

The intensity of sound in the atmosphere depends on the impedance of air (ρc) [Ref. 16], where ρ is the air density (kg/m^3) and c is the speed of

sound (m/s). These variables change with altitude, since ρ depends on pressure and temperature, c depends only on temperature, and both the temperature and pressure vary with altitude. At higher altitudes and lower temperatures, the array transducers are less efficient than they are at sea level. This does not present a problem if the echosounder calibration and its subsequent use in measurements are conducted at the same density. However, if calibration and operation are done at different altitudes, the results will not be accurate. The existing acoustic sounder program does not compensate for the change in transducer efficiency with atmospheric impedance, ρc.

Figure 8 shows the experimental equipment arrangement used to determine the echosounder's altitude dependence. A signal pulse from a HP3314A Function Generator excited a Motorola model # KSN 1005A ceramic piezoelectric driver which was sealed inside a 3-inch diameter, 82 cm long section of PVC pipe. The same 3-inch driver received the pulsed signal reflected by the flat surface at the opposite end of the tube. A Nicolet Pro 30 Digital Analyzer measured the signal intensity. Measurements were made as a vacuum pump removed the air from the pipe over a pressure range of approximately 10-1000 mbar.

A plot of the received signal voltage versus pressure should be linear if the signal amplitude is proportional to ρc. This relationship provides an altitude correction to the anechoic calibration. The AEOS Hawaii observatory at 3 km altitude has a pressure that is 30% lower than at sea level.

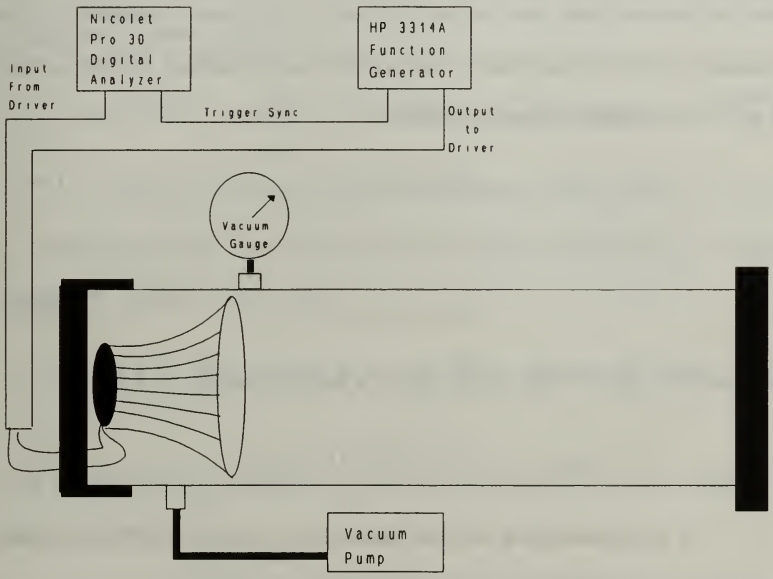

Figure 8. One driver pressure dependence measurement equipment set-up.

4. Modified Echosounder Equation

Assume that an echosounder transducer produces a peak on-axis intensity, at a distance r, given by

$$I_0 \left(\frac{r_0}{r}\right)^2 \left(\frac{W}{m^2}\right) \quad . \tag{18}$$

Here we assume that the far-field intensity, $I_0(r_0)$ was measured in the laboratory at a known distance r_0. Using the far field amplitude antenna pattern $F(\theta,\phi)$, the normalized intensity is then

$$|F(\theta,\phi)|^2 \quad , \tag{19}$$

where

$$|F(0,0)|^2 \equiv 1 \quad . \tag{20}$$

Consequently, the far-field irradiance on a target at range r will be

$$I_{target} = I_0 \left(\frac{r_0}{r}\right)^2 |F(\theta,\phi)|^2 \left(\frac{W}{m^2}\right) \quad . \tag{21}$$

If the atmospheric volume backscatter coefficient at some angle ζ with respect to the incident sound direction is

$$\sigma(\zeta) \quad (m\ steradian^{-1}) \quad , \tag{22}$$

the power scattered by σ is

$$dP_s(\zeta) = I_t \sigma(\zeta)\, dV \ (W/sr) \quad , \tag{23}$$

where the ensonified volume element of area da, for a pulse length τ and speed of sound c is

$$dV = \frac{c\tau}{2} da \ (m^3) \quad . \tag{24}$$

The scattered power is then

$$dP_s(\theta,\phi,\zeta) = I_0 \left(\frac{I_0}{r}\right)^2 |F(\theta,\phi)|^2 \sigma(\zeta) \frac{c\tau}{2} da \ (W/sr) \quad . \tag{25}$$

A receiver antenna of area A will subtend a solid angle of A/r^2 from the scattering volume. So the backscattered power received at $\zeta = \pi/2$ also depends on $|F(\theta,\phi)|^2$ and will be

$$dP_r(\theta,\phi) = I_0 \left(\frac{I_0}{r}\right)^2 |F(\theta,\phi)|^2 \sigma(\pi/2) \frac{c\tau}{2} da \frac{A}{r^2} |F(\theta,\phi)|^2 \ (W) \quad . \tag{26}$$

Using $d\Omega = da/r^2$ and regrouping the antenna pattern terms, the backscattered power becomes

$$dP_r(\theta,\phi) = I_0 r_0^2 \sigma(\pi/2) \frac{c\tau}{2} \frac{A}{r^2} |F(\theta,\phi)|^4 d\Omega \ (W) \quad . \tag{27}$$

Dividing by A, the area of the antenna, we can rewrite this in terms of the irradiance at the receiver

$$dI_r(\theta,\phi) = I_0 \frac{I_0^2}{r^2} \sigma(\pi/2) \frac{c\tau}{2} |F(\theta,\phi)|^4 d\Omega \left(\frac{W}{m^2}\right) \quad . \quad (28)$$

Integrating over the solid angle illuminated by the antenna and including the round trip absorption loss for an attenuation coefficient, α, gives

$$I_r = I_0 \frac{I_0^2}{r^2} \sigma(\pi/2) \frac{c\tau}{2} e^{-2\alpha r} \int_0^{\Omega_1} |F(\theta,\phi)|^4 d\Omega \left(\frac{W}{m^2}\right) \quad . \quad (29)$$

This formulation allows us to use a laboratory calibration of the receiver sensitivity expressed in terms of mV/Pa, which will then be converted to Watts using 20×10^{-6} Pa $\rightarrow$ 1×10^{-12}W. The solid angle covered by the integral should include only the main lobe, since the array enclosure suppresses the sidelobes.

Compare this with the previous NOAA formulation of Little, Hall or Neff

$$\frac{P_R}{E_R} = [P_T E_T] [e^{-2\alpha R}] [\sigma_o(R,f)] [\frac{c\tau}{2}] [\frac{A}{R^2} G] \quad . \quad (30)$$

Although similar to the expression above, there are significant differences. Here the terms P_t, E_t and E_r as well as G are virtually impossible to determine since they depend on the antenna beamwidth as well as the transducer conversion efficiencies. The G term is not the antenna gain but is related to the $F(\theta,\phi)$ integral. This equation uses the total power P_T a difficult to determine parameter compared to the peak on axis irradiance.

IV. EXPERIMENTAL RESULTS

A. RECEIVING EFFICIENCY

A B&K Type 4228 pistonphone calibrated the 1/4", B&K calibrated microphone (serial # 1181490). The factory calibration of the pistonphone was 124.15 dB for a reference signal of 20 μPa. Converting acoustic intensity to pressure gives

$$[10^{(\frac{124.15dB}{20})}][20x10^{-6}\,Pa] = 32.2\pm.2\,Pa_{RMS} \quad ,$$

for the signal produced by the pistonphone. The microphone produced a signal amplitude of $103.7\pm.5$ mV_{RMS} using the pistonphone and an HP 3561A Signal Analyzer. The calibration coefficient, C_{piston}, was calculated by dividing the microphone measurement by the pressure generated by the pistonphone

$$C_{piston} = \frac{103.7\,mV}{32.25\,Pa} = 3.22\pm.02\,\frac{mV}{Pa} \quad .$$

The open circuit amplitude of the signal received by the array was found to be $504.7\pm.5$ μV_{RMS}, for a 1.0 V signal input to a 1-inch dime tweeter 5.25 m from the array. The array was then replaced with the calibrated microphone. The microphone signal amplitude was $24.8\pm.5$ μV_{RMS}.

Equation (5) states that the array receiving efficiency, E_R, should specify the efficiency for conversion of acoustic power back to electrical power. This

is a deceptive, and probably erroneous concept since the array is a transducer that produces a voltage from an applied pressure. The 21.1 ohm impedance array feeds a high impedance amplifier (1 MΩ). The amplifier receives very little power since the electrical impedances are not matched. One is tempted to compute the electrical power produced from the acoustic power with

$$P_R = \frac{V^2_{RMS}}{Z}$$

where Z = 21.1 ohms is the electrical impedance of the array, but this is incorrect. Instead, the receiving efficiency must be specified in terms of the open circuit voltage produced per unit pressure, V/Pa, as is done for calibrating microphones. The array produced a signal of $24.8 \pm .5\ \mu V_{RMS}$. Since the microphone calibration factor was 3.22 mV/Pa, the array receiving sensitivity was

$$C_{rec} = \frac{504.7\ \mu V}{24.8\ \mu V} \cdot (3.22 \frac{mV}{Pa}) = 65.5 \pm 1.3\ (\frac{mV}{Pa}) \quad .$$

After measuring the received voltage this constant allows us to compute the equivalent pressure and then the power using the relationship 20×10^{-6} Pa → 1×10^{-12} W/m^2.

B. TRANSMITTING EFFICIENCY

The 1/4 inch, B&K calibrated condenser microphone (serial # 1181490) was calibrated with the pistonphone as before, in the previous

section, but for a slightly lower ambient atmospheric pressure (1013.0 mbar). The pistonphone factory calibration was 124.08 dB for a reference signal of 20 μPa. Converting this intensity to pressure gives

$$[10^{(\frac{124.08\,dB}{20})}]\,[20 \times 10^{-6}\,Pa_{RMS}] = 31.99\,Pa_{RMS}$$

the signal produced by the pistonphone. The HP 3561A Signal Analyzer measured a signal amplitude of 97.95 mV_{RMS} when the microphone was inserted in the pistonphone. The calibration coefficient, C_{piston}, was 3.062 mV/Pa.

Figure 9 shows the two axes of symmetry for the hexagonal array. The array characteristics were measured along both axes of symmetry. TABLE I shows the signal amplitudes measured by the calibrated microphone. Four measurements were recorded at each position, two side-mounted and two apex-mounted.

The measured voltages were then converted into power densities using Equations (10) through (13). The total power contained in the main lobe was calculated using Equations (14) through (17). TABLE II shows the measured power in the main lobe for each array orientation. The measurements for the side mounted array were greater than the apex mounted because of the difficulty in aligning the array maximum peak with the microphone. The average total lobe power, P_{total}, was $(3.0 \pm .3) \times 10^{-4}$ W.

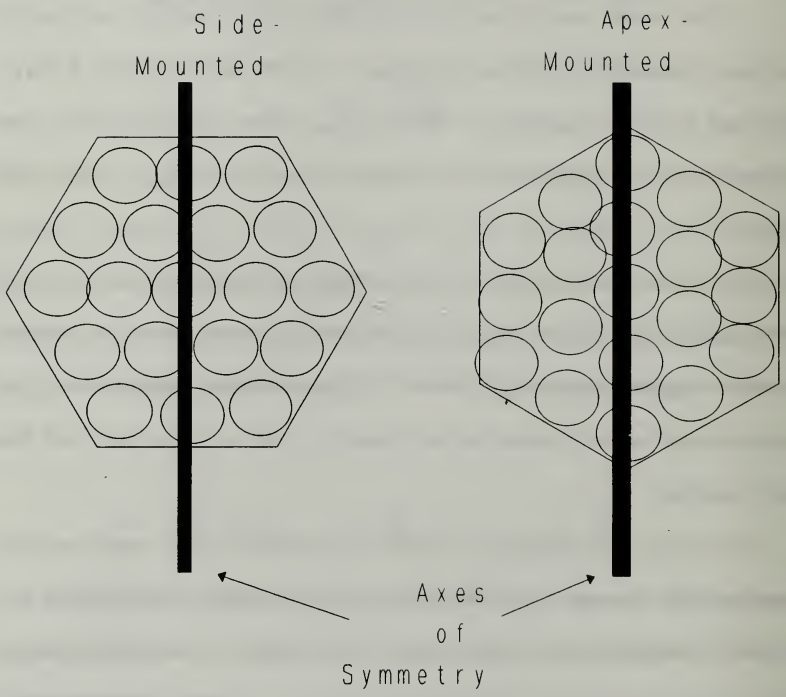

Figure 9. Power density measurements of the hexagonal array were made along both axes of symmetry.

TABLE I. SIGNAL AMPLITUDES MEASURED AT DISTANCES INDICATED FROM MAIN LOBE CENTROID.

Distance from Centroid (m)	Array Orientation			
	SIDE Mounted (mVrms)		**APEX** Mounted (mVrms)	
	Run #1	Run #2	Run #3	Run #4
0.0	1.370	1.374	1.345	1.335
0.05	1.292	1.292	1.291	1.298
0.10	1.288	1.276	1.247	1.253
0.15	1.265	1.258	1.145	1.225
0.20	1.208	1.192	1.176	1.182
0.25	1.163	1.150	1.081	1.072
0.30	1.072	1.057	1.002	1.027
0.35	0.9772	0.9716	0.9268	0.934
0.40	0.9495	0.9457	0.8770	0.883
0.45	0.8785	0.8872	0.8366	0.828
0.50	0.7975	0.7713	0.7100	0.719
0.55	0.6649	0.6618	0.5791	0.580
0.60	0.6166	0.6095	0.5245	0.533
0.65	0.5728	0.5669	0.5079	0.504
0.20	0.4756	0.4626	0.4323	0.430
0.25	0.4276	0.4210	0.3272	0.317
0.30	0.3569	0.3471	0.2397	0.253
0.35	0.2371	0.2432	0.2074	0.216
0.90	0.2308	0.2301	0.1382	0.142
0.95	0.1957	0.1972	0.1453	0.103
1.00	0.1235	0.1218	0.0506	0.038
1.05	0.0606	0.0692	0.0393	0.051
1.10	0.0549	0.0545		
1.15	0.0463	0.0306		

TABLE II. TOTAL POWER CALCULATED IN MAIN LOBE FOR EACH ARRAY ORIENTATION.

Array Orientation			
SIDE Mounted Total Power (W)		**APEX** Mounted Total Power (W)	
Run #1	Run #2	Run #3	Run #4
0.000328	0.000323	0.000270	0.000273

The input power applied to the array is a product of the RMS current and voltage applied to the array and the cosine of the phase angle. An HP4194A Complex Impedance Analyzer found the phase angle to be θ = -46.8 degrees at 5000 Hz. Since the input current was 0.010 A_{RMS} for a voltage of 208.8 mV_{RMS}, the array input power P_{input} was $(1.43 \pm .01) \times 10^{-3}$ W. The transmitting efficiency, E_T, was 21 ± 2 percent. This is significantly lower than the 50 percent that Weingartner [Ref 2] estimated and was used in the echosounder program. Substituting this value for E_T into Equation (7) would increase the recorded C_n^2 values by a factor of 2.

C. ALTITUDE DEPENDENCE

The HP3314A function generator generated a 1 volt, 5 kHz, 10 cycle signal burst which was both transmitted and received by the same 3-inch driver inside a sealed section of PVC pipe. TABLE III shows the sound intensities received by the 3-inch driver as the air was pumped out of the sealed PVC pipe.

The sound intensities were plotted versus air pressure. Figure 10 shows the sound intensity dependence on pressure with a polynomial best fit superimposed over the data plot.

Sound pressure readings can be extracted from Figure 10 when the applicable air pressure is known. The air pressure at sea level is approximately 1013 mbar. At the Starfire Optical Range (SOR) it is approximately 810 mbar, while the Advanced Electro-Optic Site (AEOS) has an air pressure of approximately 700 mbar. These pressures translate to sound voltages received of 44.84 mV (sea level), 42.96 mV (SOR) and 40.74 mV (AEOS) for an identically transmitted 1.0 V, 5.0 kHz signal. This pressure dependence must be factored into the echosounder calibration before it can be applied to the AEOS data.

TABLE III. SIGNAL INTENSITY MEASUREMENTS RELATIVE TO AIR PRESSURE

Pressure (mbar)	Signal Intensity (mV)	Pressure (mbar)	Signal Intensity (mV)
10.73		471.28	33.16
14.12		505.14	34.8
31.05	0.9	539.01	36.06
47.98	2.04	572.87	36.8
64.91	3.18	606.73	37.8
81.84	4.62	640.6	39.1
98.78	6.06	674.46	40.01
132.64	9.46	708.33	41.06
166.5	12.6	742.19	41.65
200.37	16.0	776.05	42.52
234.23	19.06	809.92	42.94
268.09	21.5	843.78	43.3
301.96	23.34	877.64	43.52
335.82	26.1	911.51	43.92
369.69	27.6	945.37	44.25
403.55	30.18	979.24	44.94
437.41	31.6	1013.1	44.84
454.35	32.38		

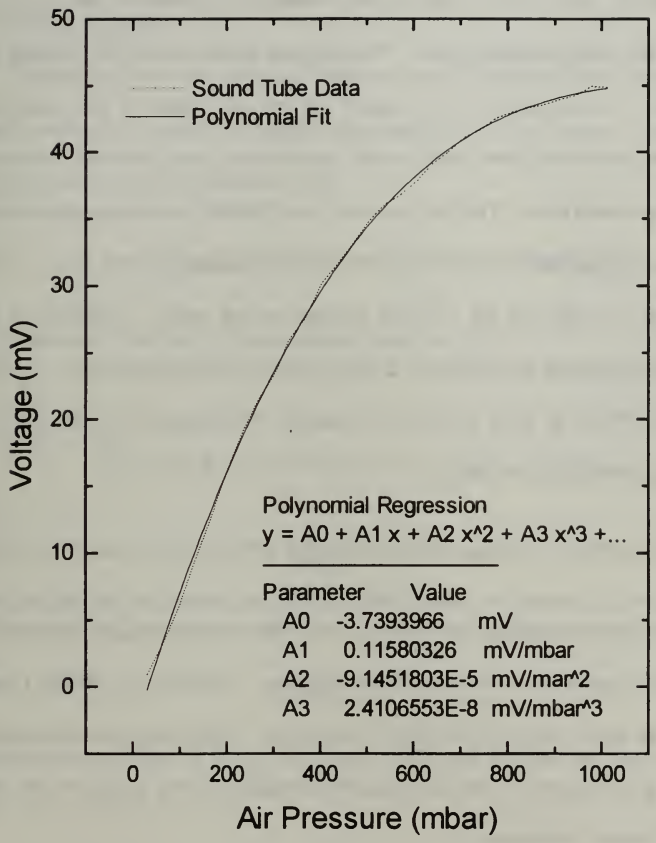

Figure 10. Signal intensity dependence on air pressure with polynomial fit superimposed on data plot.

D. MODIFIED ECHOSOUNDER EQUATION

Measurements of the peak sensitivity of the array were very sensitive to alignment of the array since small angular misalignments moved the maximum away from the measurement point. The highest values in TABLE I reveal this phenomena. Consequently, the higher values of TABLE I, the first two columns, are probably more reliable than the second two columns that have some misalignment error. The first column from TABLE I shows a peak on axis microphone voltage of 1.37 mV for 0.208 mV applied to the array. This corresponds to 6.49 mV for 1.0 volt applied to the array. Dividing by the calibrated microphone sensitivity of 3.062 mV/Pa, this corresponds to 2.12 Pa or 1.12×10^{-2} W/m^2 at 5.25 m from the source. Referencing this to 1 m the transmitting efficiency becomes

$$C_{trans} = 0.309 \left(\frac{W}{(Vm)^2}\right) \quad .$$

Calculating the average transmitting/receiving antenna angular distribution over the main beam lobe was a bit more involved. The data of TABLE I were normalized so that $F(0,0) = 1$ and $d\Omega = \sin\theta \, d\theta \, d\phi$. The integral was simplified by assuming symmetry in the ϕ direction and using θ_1 the angle of the first diffraction pattern minimum,

$$\int_0^{\Omega_1} |F(\theta,\phi)|^4 \, d\Omega = \int_0^{\theta_1}\int_0^{2\pi} |F(\theta)|^4 \sin\theta \, d\theta \, d\phi = 2\pi \int_0^{\theta_1} |F(\theta)|^4 \sin\theta d\theta \ .$$

Using Simpson's method the integral was evaluated numerically and found to be $0.0096 \pm .0004$.

Recalling the transmitting efficiency of 0.309 W/(Vm)^2 (at 1 m and 1 V_{RMS}) and the angular integral of 0.0096 (rounded off to 0.01) allows us to compare the previously stated Equation (29)

$$I_r = I_0 \frac{{I_0}^2}{r^2} \sigma(\pi/2) \frac{c\tau}{2} e^{-2\alpha r} \int_0^{\Omega_1} |F(\theta,\phi)|^4 \, d\Omega \ (\frac{W}{m^2}) \ , \qquad (29)$$

with the older calibration expression, Equation (30)

$$\frac{P_R}{E_R} = [P_T E_T] \ [e^{-2\alpha R}] \ [\sigma_o(R,f)] \ [\frac{c\tau}{2}] \ [\frac{A}{R^2} G] \ . \qquad (30)$$

Dividing Equation (30) by the antenna area, A, and eliminating like terms in both equations, allows us to compare the sound intensities, I_r, at r = 1 m

$$\frac{P_R}{A E_R} = P_T E_T G \ .$$

Substituting values for V_{RMS}, (25 V), E_T (0.5) and G (0.4) we have

$$\frac{(25\ V)^2}{21\ \Omega} \cdot (0.5) \cdot (0.4) = 6.0 \ (\frac{W}{m^2}) \ ,$$

for the transmitted sound intensity. This intensity was multiplied by the receiving efficiency, E_R, array area, phase angle and the impedance (21 Ω) to find the received V^2

$$6.0\ (\frac{W}{m^2}) \cdot (0.5) \cdot (0.0866\ m^2) \cdot \cos(-46.8°) \cdot (21\ \Omega) = 3.76\ (V^2) \quad ,$$

for comparision with the modified echosounder equation.

For Equation (29), using r_o = 1 m, we have

$$I_o = C_{trans} \cdot V_{RMS}^2 \int_0^{\Omega_1} |F(\theta,\phi)|^4\, d\Omega \quad .$$

Substituting values for C_{trans} (0.309), V_{RMS} (25 V) and the angular integral (0.01), we have

$$0.309\ (W/(Vm)^2) \cdot (25\ V)^2 \cdot 0.01 = 1.93\ (\frac{W}{m^2}) \quad ,$$

for the transmitting sound intensity. A receiving conversion coefficient was found using the receiving sensitivity (65.5 mV/Pa), mentioned earlier, and the pressure-to-intensity conversion i.e.,

$$C_{rec} = (\frac{6.55x10^{-2}\ V}{20x10^{-6}})^2 = 1.72\ (\frac{V^2}{W/m^2}) \quad .$$

The transmitting voltage was multiplied by the receiving conversion coefficient, the area of the array and the phase angle to give the receiving V^2 for comparison

$$1.93\left(\frac{W}{m^2}\right)\cdot 1.72\left(\frac{V^2}{W/m^2}\right) = 3.32\,(V^2) \quad .$$

Comparing these two expressions we find that they are approximately equal. Since both of these approaches result in the same approximate value, it is not clear why a factor of four discrepancy between the echosounder and microthermal probe values exists.

V. CONCLUSIONS AND RECOMMENDATIONS

A. CONCLUSIONS

To date, most acoustic echosounders have used an expression for computing C_T^2 and optical turbulence that contain transducer total power and efficiency terms P_T, E_T, E_R, and G that depend on the transducer electrical-acoustic efficiencies as well as the antenna beam pattern coupled together. This coupling has made calibration exceedingly difficult. To avoid this problem, this thesis research considered two separate calibration approaches. The first was to measure C_T^2 directly using microthermal probes on a tower and compare these results with the acoustic sounder measurements. The second approach was to recast the calibration problem into separate transducer transmitting and receiving calibration coefficients measured in an anechoic chamber. These calibrations include the work of Probert-Jones that state that a monostatic radar must include an average over the product of the transmitting and receiving antenna beam patterns leading to an integral over the forth power of the antenna amplitude angular distribution.

The September 1992 tower measurements showed that the original acoustic sounder calibration expression overestimated the actual atmospheric turbulence by a factor of four. This factor of four had been seen in previous work, but the source of this factor was not clear.

Using the acoustic calibration procedure in an anechoic chamber the transmitting coefficient was 0.309 W/(Vm^2) at 1 m for each volt RMS applied to the array. The receiving sensitivity was 65.5 ± 1.3 mV/Pa. Combining these two coefficients produced results that were nearly identical with the previous calibration expression. To date these coefficients have failed to resolve the factor of four discrepancy between the acoustic calibration measurements and calibration measurements performed using microthermal probes.

This thesis also investigated the dependence of the acoustic echosounder calibration on the acoustic impedance of the air, ρc, which varies with atmospheric temperature and pressure. Although a ρc decrease of 30 percent was expected from sea level to 3 km, the actual driver measurements found a 9 percent reduction. These occurred since the acoustic drivers operated at resonance and the displacement of air around the driver horn phasing plug provided considerable damping. This damping declined with reduced air pressure leaving the driver displacement relatively unchanged.

We consider the tower calibrations to be the most accurate at this time since they are consistent with previous turbulence measurements. The inconsistency between the microthermal probe and acoustic calibrations remains intriguing.

B. RECOMMENDATIONS

The factor of four discrepancy between the acoustic and microthermal echosounder calibrations needs to be resolved. The source of this could be as simple as (an elusive) programming error. Although this has been examined, carefully, the potential for such an error exists. On the other hand, this discrepancy may indicate a more fundamental problem with the theoretical expressions relating atmospheric turbulence to the acoustic scattering cross-section or that atmospheric turbulence in the 3 cm size range is four times larger than expected. Another possibility is that the micothermal reference probes are in error by a factor of four.

LIST OF REFERENCES

1. Walters, D.L. and Kunkel, K.E., "Atmospheric Modulation Transfer Function for Desert and Mountain Location: The Atmospheric Effects on r_0," *Journal of the Optical Society of America,* Vol. 71, April 1981.

2. Weingartner, F.J., *Development of an Acoustic Echosounder for Detection of Lower Level Atmospheric Turbulence,* Master's Thesis, Naval Postgraduate School, Monterey, California, June 1987.

3. Wroblewski, M.R., *Development of a Data Analysis System for the Detection of Lower Level Atmospheric Turbulence with an Acoustic Sounder,* Master's Thesis, Naval Postgraduate School, Monterey, California, June 1987.

4. Moxcey, L.R., *Utilization of Dense Packed Planar Acoustic Echosounders to Identify Turbulence Structure in the Lowest Levels of the Atmosphere,* Master's Thesis, Naval Postgraduate School, Monterey, California, December 1987.

5. Tatarski, V.I., *Wave Propagation in a Turbulent Medium,* McGraw-Hill Book Company, Inc., New York, 1961.

6. McCary, J.K., *High Resolution C_T^2 and Radial Velocity Measurements Using a High Frequency Monostatic Acoustic Echosounder,* Master's Thesis, Naval Postgraduate School, Monterey, California, June 1990.

7. Fried, D.L., "Anisoplanatism in Adaptive Optics," *Journal of the Optical Society of America,* Vol. 72, pp. 52-61, 1982.

8. Neff, W.D., "Quantitative Evaluation of Acoustic Echoes from the Planetary Boundary Layer," *NOAA Technical Report ERL 322-WPL 38,* June 1975.

9. Little, C.G., "Acoustic Methods for the Remote Probing of the Lower Atmosphere," *Proceedings of the IEEE,* Vol. 57, June 1969.

10. Hall Jr., F.F., and Wescott, J.W., "Acoustic Antennas for Atmospheric Echo Sounding," *Journal of the Acoustical Society of America,* Vol. 56, No. 5, November 1974.

11. Mattingly, T.S., *Measurement of Surface Layer Optical Turbulence Above*

AMOS, Master's Thesis, Naval Postgraduate School, Monterey, California, December 1991.

12. Bourne, I.A., "Acoustic Instrumentation and Techniques for Atmospheric Studies," paper presented at the International Symposium on Acoustic Remote Sensing Of the Atmosphere and Oceans, 1st, University of Calgary, Calgary, Alberta, Canada, 22-25 June 1981.

13. Probert-Jones, J.R., "The Radar Equation in Meteorology," a manuscript submitted to the Department of Meteorology, Imperial College, London, England, January 1962.

14. Greenwood, D.P., Haugen, D.A., Kellen, P.F., "AMOS Seeing Quality Measurements," *Rome Air Development Center Report RADC-TR-75-295,* January 1976.

15. Gast, V.J., *Characterization of Atmospheric Turbulence for High Resolution Imaging and Laser Propagation Objectives,* Master's Thesis, Naval Postgraduate School, Monterey, California, December 1992.

16. Kinsler, L.E., Frey, A.R., Coppens, A.B., and Sanders, J.V., *Fundamentals of Acoustics,* John Wiley & Sons, Inc., New York, 1982.

INITIAL DISTRIBUTION LIST

1.	Defense Technical Information Center Cameron Station Alexandria, VA 22304-6145	2
2.	Library, Code 52 Naval Postgraduate School Monterey, CA 93943-5002	2
3.	Professor Karlheinz E. Woehler Chairman, Department of Physics Naval Postgraduate School (Code PHWh) Monterey, CA 93943	1
4.	Professor Donald L. Walters Naval Postgraduate School (Code PHWe) Monterey, CA 93943	4
5.	U.S. Air Force Geophysics Directorate Phillips Lab (GPOA) ATTN: Bob Beland Hanscom AFB, MA 01731-5000	1
6.	U.S. Air Force Phillips Laboratory (PL/LI) ATTN: Richard Frosch Kirtland, AFB, NM 87117	1
7.	U.S. Air Force Phillips Laboratory (PL/LI) ATTN: Larry Weaver Kirtland, AFB, NM 87117	1
8.	U.S. Air Force Phillips Laboratory (PL/LI) ATTN: Barry Hogge Kirtland, AFB, NM 87117	1
9.	US Army Nuclear & Chemical Agency ATTN: MAJ David R. Cherry Fort Belvoir, VA 22060	2